Journal of Luminescence 247 (2022) 118854

Contents lists available at ScienceDirect

Journal of Luminescence

journal homepage: www.elsevier.com/locate/jlumin

Luminescence nanothermometry via white light emission in Ho^{3+}, Tm^{3+}: Y_2O_3 colloidal nanocrystals

Albenc Nexha, Maria Cinta Pujol *, Joan Josep Carvajal, Francesc Díaz, Magdalena Aguiló

Universitat Rovira i Virgili, Departament Química Física i Inorgànica, Física i Cristal·lografia de Materials i Nanomaterials (FiCMA-FiCNA), Campus Sescelades, E-43007, Tarragona, Spain

ARTICLE INFO

Keywords:
Colloidal nanocrystals
Yttrium oxide
Lanthanide doping
White light emission
Luminescence nanothermometry

ABSTRACT

Cubic Ho^{3+} and Tm^{3+} doped Y_2O_3 colloidal nanotriangles with lateral length sizes ~43 nm, were synthesized *via* thermal decomposition methodology. These colloidal nanocrystals, upon high power excitation at 808 nm, generate white light. The crystalline structure, size and shape, and the surface of the colloidal nanocrystals, were investigated before and after being exposed to laser excitation. Factors that might affect the generation of white light, such as the power of excitation source, the stability of the emission with time, and the temperature at which the colloidal nanocrystals were exposed, are analyzed. The white light displayed temperature-dependence optical properties, allowing the application of these nanocrystals as luminescent nanothermometers over a wide range of temperatures, from room temperature to 473 K. The relative thermal sensitivity and the temperature resolution of these luminescent nanothermometers are 3.38% K^{-1} and 0.15 K, respectively, at 473 K, enabling to demonstrate a new highly sensitive mechanism for luminescence thermometry.

1. Introduction

White light emitters are at the core of a broad range of applications, including solar energy conversion technologies, lighting sources, backlight, full-color displays and biomedical imaging [1–4]. Diverse materials have been reported as white light emitters, including quantum dots [5–8], semiconductor nanocrystals [9–11], small organic molecules [12–14], polymers [15–18], lanthanide complexes [19–22], and lanthanide doped inorganic materials [23–30].

Due to high luminescence efficiency and high thermal stability of the lanthanide materials (either embedded in a crystalline or amorphous host, or as part of organometallic complexes), the generation of the white light by these materials has attracted the curiosity of the scientific community. Rare earth oxides (RE_2O_3) portray, probably, the widest investigated materials to generate white light, including Y_2O_3 [24, 31–34], Er_2O_3 [35–37], Yb_2O_3 [38,39], Gd_2O_3 [40,41], La_2O_3 [42], Sm_2O_3 and Tm_2O_3 [38], PrO_2 and TbO_2 [43]. In addition, RE_2O_3 have also potential for applications in bioimaging [44–46], diagnosis and therapy [46–48], and sensing [49–51].

Nevertheless, the mechanism of the generation of white light in rare earth materials, continues to be a subject of discussion [4]. Mechanisms such as photon avalanche [30,52], oxygen vacancy emission [53], electron-hole recombination [54], dispersive optical bistability [55,56], and blackbody radiation [3,43,52,57], have been proposed. However, there is, not yet, a general agreement on what triggers the production of white light in the rare earth emitters [4]. Additional factors that might affect the white light emission, involve parameters such as the stability of the white emission with time, power of the excitation source applied, and the temperature on which the emitting materials are exposed to Ref. [4].

We have chosen yttrium oxide based materials to investigate their capability as white light emitters, mainly due to their broad transparency range (0.2–8 μm) with a band gap of 5.6 eV, high thermal conductivity, high refractive index and low phonon energy, which have convert it, traditionally, in a suitable choice as host material for lanthanide ions in optical applications [58,59]. We doped these materials with Ho^{3+} and Tm^{3+} ions. It is believed that dopants can facilitate the generation of the white light and enhance its brightness by reducing its thermal conductivity [60–62], besides of activating energy transfer processes from the doping ions to the hosts.

If the optical properties of a material are temperature-dependent, the material can act as luminescent thermometer [63]. White light emitters do display temperature-dependence properties [23,24,64]. A broad band white emission, named thermal radiation (although mechanism

* Corresponding author.
E-mail address: mariacinta.pujol@urv.cat (M.C. Pujol).

https://doi.org/10.1016/j.jlumin.2022.118854
Received 20 July 2021; Received in revised form 22 March 2022; Accepted 23 March 2022
Available online 2 April 2022

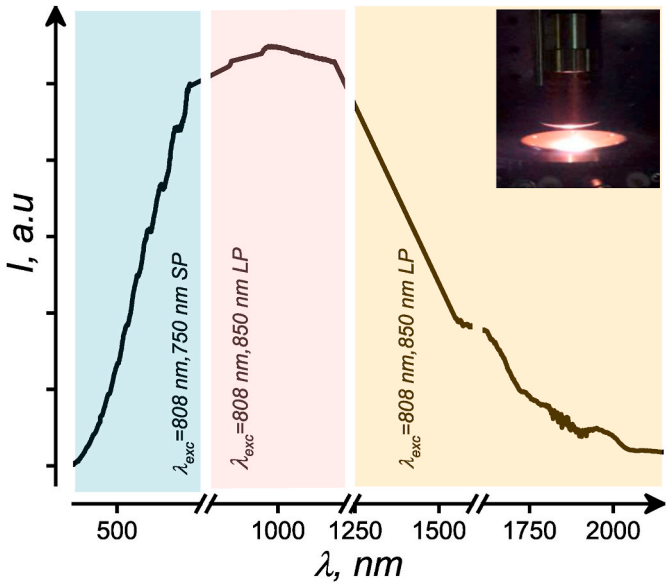

Fig. 1. Emission generated by the Ho^{3+}, Tm^{3+}:Y_2O_3 nanotriangles in the 400–2200 nm spectral range, after excitation at 808 nm with a power of 0.6 W. The inset displays a picture of the white light generated. The different intervals of collection of the spectrum are marked, SP stands for shortpass filter, and LP for longpass filter used to avoid the excitation laser signal. The signals arising from the laser (around 800 nm and 1600 nm) are removed. The detector change from Yokogawa AQ6373 (operating between 400 nm and 1200 nm) to Yokogawa AQ6375 (operating between 1250 and 2400 nm) is also removed (the break in between 1200 and 1250 nm).

still under debate [4]), is applied to extract thermal knowledge. Different methods are implemented in order to measure the temperature *via* white light: direct application of the Planck's law by a ratiometric method [23], adapting a ratiometric range within the wide band of the white light emission [24], or combining two emissions arising from two different mechanisms (the 4f-4f electronic transition of Nd^{3+} ions *versus* the broad band coming from the host [64]).

Here, we explore the ability of highly monodispersed oleic acid coated cubic Ho^{3+} and Tm^{3+} doped Y_2O_3 colloidal nanotriangles to generate white light under excitation at near infrared (NIR) 808 nm wavelength. Factors affecting the white light emission, including the power of the laser applied, its stability with time, the temperature on which the emitters are exposed, are analyzed. Taking advantage of the temperature-dependent optical properties of the white light, we explored the possibility of using these colloidal nanotriangles for luminescence nanothermometry, obtaining values of relative thermal sensitivity and temperature resolution of 3.38% K^{-1} and 0.15 K, respectively, at 473 K, indicating that these materials act as highly sensitive luminescent nanothermometers.

2. Experiments

2.1. Materials

Yttrium acetate hydrate ($Y(CH_3CO_2)_3{\cdot}H_2O$ as $Y(Ac)_3{\cdot}H_2O$, purity 99.99%) and oleylamine ($C_{18}H_{35}NH_2$, as OLAM, purity 70%) were purchased from Sigma Aldrich. Thulium acetate hydrate ($Tm(CH_3CO_2)_3{\cdot}H_2O$ as $Tm(Ac)_3{\cdot}H_2O$, purity 99.99%) was purchased from Apollo Scientific. Holmium acetate hydrate ($Ho(CH_3CO_2)_3{\cdot}H_2O$ as $Ho(Ac)_3{\cdot}H_2O$, purity 99.99%)), oleic acid ($CH_3(CH_2)_7CH = CH(CH_2)_7COOH$, as OLAC, purity 90%), 1-octadecene ($CH_3(CH_2)_{15}CH = CH_2$ as ODE, purity 90%), n-hexane (99%) and sodium nitrate ($NaNO_3$, 99%) were purchased from Alfa Aesar. Absolute ethanol (EtOH) was purchased from VWR Chemicals.

2.2. Synthesis of Ho^{3+} and Tm^{3+} doped Y_2O_3 colloidal nanocrystals

Thermal decomposition was applied to synthesize Ho^{3+} and Tm^{3+} doped Y_2O_3 colloidal nanocrystals in the shape of nanotriangles, following a previously reported methodology with slight modifications [65]. In a typical thermal decomposition synthesis of 3 mol% Ho^{3+} and 5 mol% Tm^{3+} doped Y_2O_3 colloidal nanotriangles, 2.3 mmol of $Y(Ac)_3{\cdot}H_2O$, 0.075 mmol of $Ho(Ac)_3{\cdot}H_2O$, 0.125 mmol of $Tm(Ac)_3{\cdot}H_2O$ and 4 mmol of $NaNO_3$, were mixed in a solution containing 25 mmol of OLAC, 25 mmol of OLAM and 15 mmol of ODE. The reaction mixture was heated to 413 K and degassed to remove residual oxygen for 0.5 h. After switching to nitrogen flow, the reaction temperature was increased to 583 K and held at this temperature for an additional 0.5 h, prior to letting it cool down naturally to room temperature. The nanotriangles were extracted by adding an excess of EtOH, followed by centrifugation at 5000 rpm for 10 min and redispersion in n-hexane. This purification cycle was repeated until the discarded supernatant was colorless. The final product of the reaction can be either stored as a solution by dispersing in an apolar solvent (n-hexane) or as powder by evaporating the liquid.

2.3. Characterizations

X-ray powder diffraction (XRPD) measurements were made using a Siemens D5000 diffractometer (Bragg-Brentano parafocusing geometry and vertical θ-θ goniometer) fitted with a curved graphite diffracted-beam monochromator, incident and diffracted-beam Soller slits, a 0.06° receiving slit and a scintillation counter as a detector. The angular 2θ diffraction range was set between 5 and 70°. The data were collected with an angular step of 0.05° at 3 s per step. The sample was rotated to increase the statistics of the signal collected. Cu K_α radiation was obtained from a Copper X-ray tube operated at 40 kV and 30 mA.

For the morphological characterization, transmission electron microscopy (TEM) images were recorded using a JEOL JEM-1011 electron microscope operating at an accelerating voltage of 100 kV. For the preparation of the TEM grids, the nanocrystals were dispersed in n-hexane, and around 7 μL of the diluted dispersion were drop casted on the surface of a copper grid covered by a holey carbon film (HD200 Copper Formvar/Carbon).

Fourier Transform Infrared (FT-IR) spectra were recorded in the range of 400–4000 cm^{-1} on a FT-IR IluminatIR II, Smith spectrophotometer, to investigate the presence of the different functional groups on the samples to determine which surfactant species are attached onto the surfaces of the nanocrystals.

The white light generated by the doped nanocrystals was recorded in a range from 400 nm to 2200 nm. The emission was recorded as three independent spectra: 400–750 nm, using a 750 nm shortpass dichroic filter (Thorlabs) to avoid the laser excitation; 850–1200 nm using an 850 nm longpass dichroic filter (Thorlabs) to avoid the laser excitation; and 1200–2200 nm using an 850 nm longpass dichroic filter (Thorlabs). The first two spectra were collected using a Yokogawa AQ6373 optical spectrum analyzer, while the last one was recorded using a Yokogawa AQ6375 optical spectrum analyzer, operating in all cases with a resolution of 2 nm and an integration time of 1 s. The nanoparticles were excited by an 808 nm fiber-coupled diode laser operating at different powers. The laser beam was focused on the sample using a 20× microscope objective (numerical aperture N.A = 0.4), generating a spot of approximately 10^{-6} m in diameter on the sample. To record the temperature-dependence of the spectra, the setup was the same, except that the nanocrystals were introduced inside a heating stage (Linkam, THMS 600) equipped with a boron disk for improved temperature distribution.

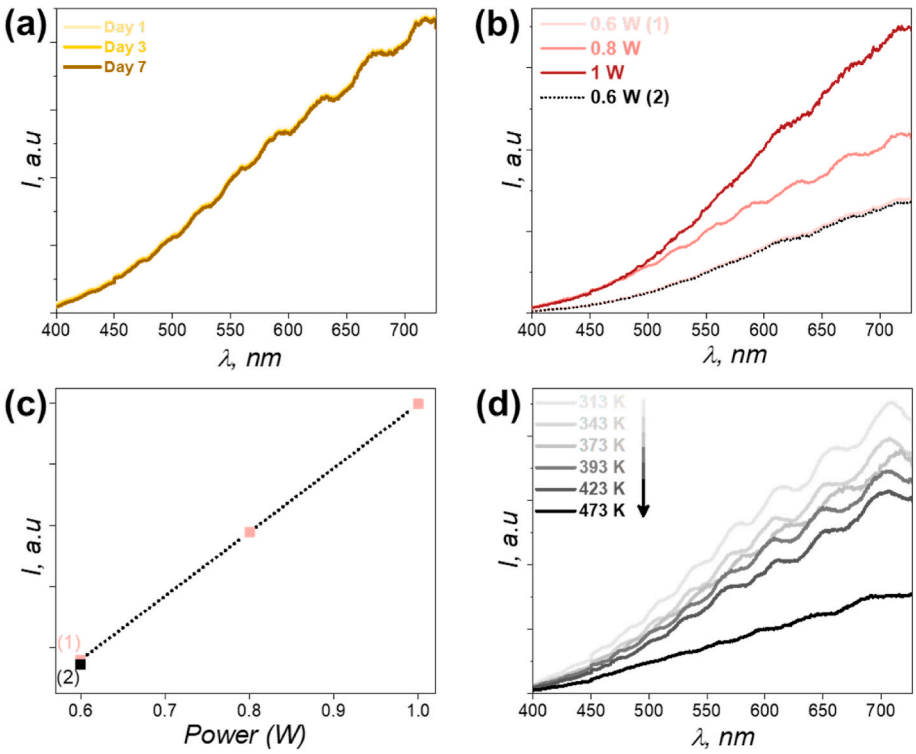

Fig. 2. The effect of: (a) time, power of the excitation source (b) on the shape of the spectra, and (c) on the intensity, and (d) temperature at which the nanocrystals were exposed, on the white light emission. Numbers (1) and (2) within (b) and (c) stand for the emissions recorded with a 0.6 W excitation power at the beginning and at the end of experiment after reaching 1 W.

3. Results and discussion

3.1. White light generated by Ho^{3+} and Tm^{3+} doped Y_2O_3 colloidal nanocrystals

3 mol% Ho^{3+}, 5 mol% Tm^{3+} doped Y_2O_3 (hereafter Ho^{3+},Tm^{3+}:Y_2O_3) colloidal nanotriangles, in powder form, were excited at 808 nm using laser power ranging from 0.6 to 1 W. This doping ratio was selected due to their brighter emissions for Ho^{3+} and Tm^{3+} ions in the NIR region, compared to other ratios, as previously described [66]. Excitation with the 808 nm laser generated white light emission in these nanocrystals. We noted that in the absence of these lanthanide ions, or *via* excitation with 980 nm laser source, we could not observe the generation of white light, hence these ions play a crucial role on triggering the white light. It is accepted that the white light emission is not specific to any oxide matrix, but is regarded rather as a general process as long as the NIR laser can be efficiently absorbed [4]. To that end, Tm^{3+} ions can efficiently absorb 808 nm laser source [66–68].

We recorded the emission over a wide range of wavelengths from 400 nm to 2200 nm but avoiding the signal of the 808 nm laser source with the corresponding filters. For that, we split the collection range into three intervals: 400–750 nm (with a 750 nm shortpass dichroic filter), 850–1200 nm (with an 850 nm longpass dichroic filter), and 1200–2200 nm (with an 850 nm longpass dichroic filter). The collected signals, after excitation with a power of 0.6 W (power density ~400 W cm^{-2}), were combined to identify the shape of the white light emission. Results, summarized in Fig. 1, reveal the shape of the white emission through all the 400 nm–2200 nm range. The emission spectra of the nanocrystals display a very broad band extending from the visible to the near infrared spectral regions. The inset in Fig. 1 illustrates a picture of the white light emission obtained, revealing its high brightness. In general, the spectral shape of the emission consists of a broad unstructured band that increase monotonically, notably in the visible range interval from 400 to 750 nm (Fig. 1). The second interval from 850 to 1200 nm displays a constant intensity of the light. The last interval, from 1200 to 2200 nm displays a decreasing profile of the white emission.

We should stress that to trigger the generation of white light and keep it stable, the nanocrystals have to be exposed to high laser powers (threshold power of 0.6 W or power density ~400 W cm^{-2}), and a temperature of around 313 K. After these pretreatments, the white light remains stable through time. Taking into account the pretreatments we have to apply, it seems that the mechanism after the generation of white light in Ho^{3+},Tm^{3+}:Y_2O_3 nanotriangles resembles that of the thermal radiation [4]. Nevertheless, as stated above, a wide variety of mechanisms have been proposed [3,30,43,52–57], and this topic is still under debate [4].

Given the high intensity of the emission generated within the visible region and the fact most of the applications for these white light emitters take profit only of the emissions located in this region [1–4], we focused our attention on this spectral region. Hence, within the 400–750 nm range, we investigated the effect of several factors, such as the stability with time, the power of the excitation source, and the temperature at which the nanocrystals were exposed, on the generated white light emission. Concerning the stability of the spectrum with time, the white light generated by Ho^{3+},Tm^{3+}:Y_2O_3 nanotriangles after 1, 3 and 7 days, recorded at an excitation power of 0.6 W, remains unchanged (Fig. 2 (a)), implying highly stable white light emission. Next, we observed the effect of the power of the 808 nm laser excitation source on the intensity of the white light. The power of the laser was increased from 0.6 W to 1 W (Fig. 2 (b)). Results indicated that it exists a proportional relationship between the emission intensity and the laser power applied (Fig. 2 (c)). In addition, we tested the stability of the white light emission by dropping the power of the laser back to 0.6 W at the end of the experiment and recording again the emission (labelled as 0.6 W (2) in Fig. 2 (b) and (c) to distinguish it from the one labelled as 0.6 W (1) recorded at the beginning of the experiment). The data show clearly that the shape (Fig. 2 (b)) and the intensity ((Fig. 2 (c)) of the emission matches the one recorded at the beginning of the experiment with the same power.

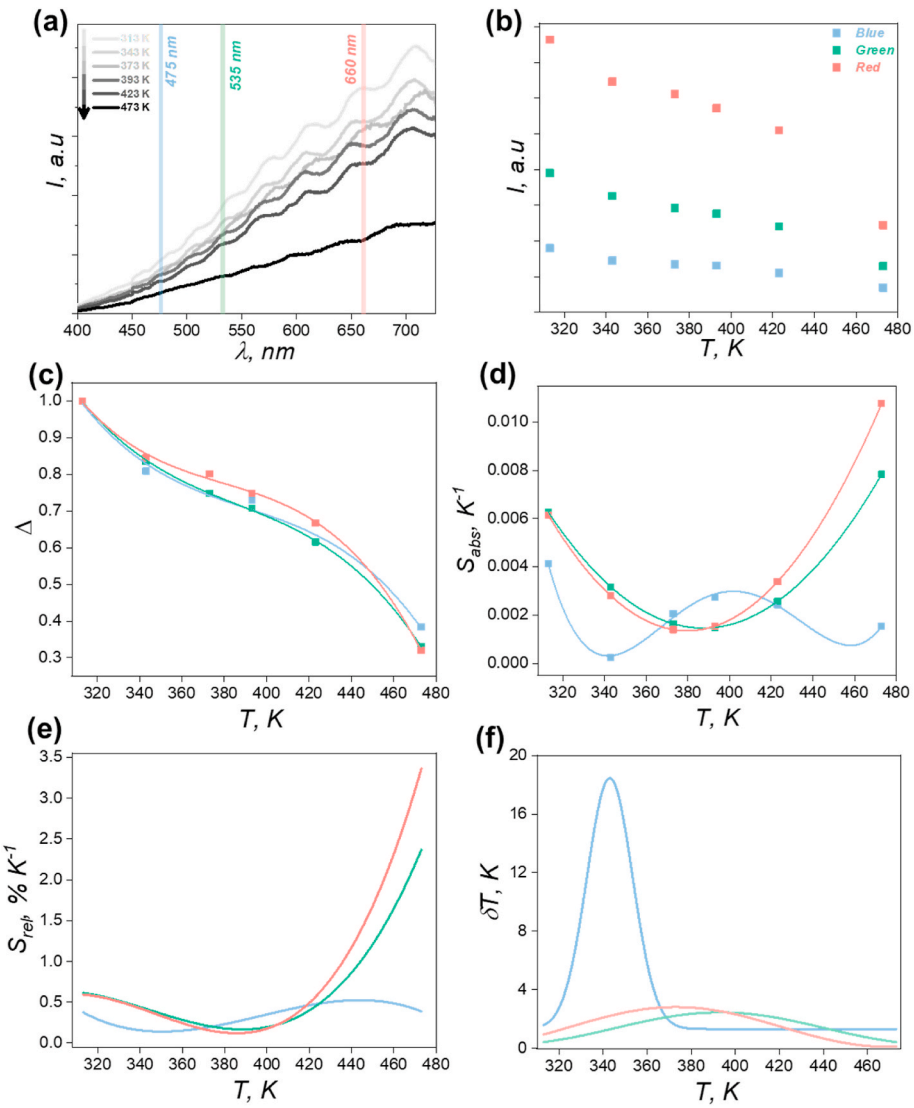

Fig. 3. (a) Temperature-dependence of the spectra and selection of the blue (475 nm), green (535 nm) and red (660 nm) wavelengths of the white light emission. Effect of the temperature in: (b) the intensity of the red, green and blue wavelengths, (c) normalized intensity evolution vs. temperature for the selected wavelengths (scattered points are experimental data and lines are fitting lines according to Equation 1), (d) absolute thermal sensitivity S_{abs}, (e) relative thermal sensitivity S_{rel}, and (f) temperature resolution δT. (For interpretation of the references to color in this figure legend, the reader is referred to the Web version of this article.)

Last, to analyze the temperature-dependence of the white light emission, the colloidal nanocrystals were introduced in a heating stage to control the temperature in the range from 313 K to 473 K. It is generally accepted that the emissions rising from rare earth doped particles are temperature-dependent [66–71], regardless of their operating range [63]. We observed that above 473 K, the white light emission was ceased. Hence, upon excitation at 808 nm with 1 W to maximize the intensity of the white light emission, we recorded the evolution of the spectra over the 400–800 nm range. Results, presented in Fig. 2 (c) indicate a clear decrease of the intensity of the white light, with a more pronounced effect above 423 K. The important dependence of the intensity of the white light emission with the temperature, allowed us to explore the possibility of using this emission for luminescence nanothermometry applications.

3.2. Luminescent nanothermometry with white light emission

To explore the application as luminescent nanothermometers of the white light emission arising from these nanotriangles in the visible, we selected three specific wavelengths in RGB (red-green-blue) region within the temperature range from 313 K to 473 K. Hence, we defined the blue wavelength at 475 nm, the green wavelength at 535 nm, and the red wavelength at 660 nm (Fig. 3 (a)). This strategy would allow us, in the future, to implement a RGB digital color sensor to develop fast, compact, low-cost and non-invasive temperature nanosensors, as we reported previously for other less efficient lanthanide doped luminescent nanoparticles with emissions in the different RGB spectral regions [72].

It can be observed in Fig. 3 (b) that as the temperature increases, the emission intensity in the red region decreased faster than in the other two regions. From its side, the emission intensity in the green region also decreased faster than in the blue region, although not as fast as the emission intensity in the red region. Last, the emission intensity in the blue region exhibits the smallest change with the temperature (Fig. 3 (b)). Thus, these characteristics indicates that we can develop a luminescent thermometer by calculating the intensity ratio of each particular wavelength as a function of temperature. We discarded the option of a ratiometric methodology as the white light emission arising from these nanotriangles is continuous, in which the intensity of different spectral regions decreases all together.

According to that, we analyzed the evolution of the intensity, Δ, normalized to the intensity at the initial temperature (313 K). The data included in Fig. 3 (c), display the temperature-dependence of the normalized intensity. Within the temperature range explored, the intensity continuously decreased as the temperature increased. As done previously in the literature [24], we applied a phenomenological fitting model to describe this variation, using a third-order polynomial fitting model (R^2 values above 0.99) for the interval from room temperature to

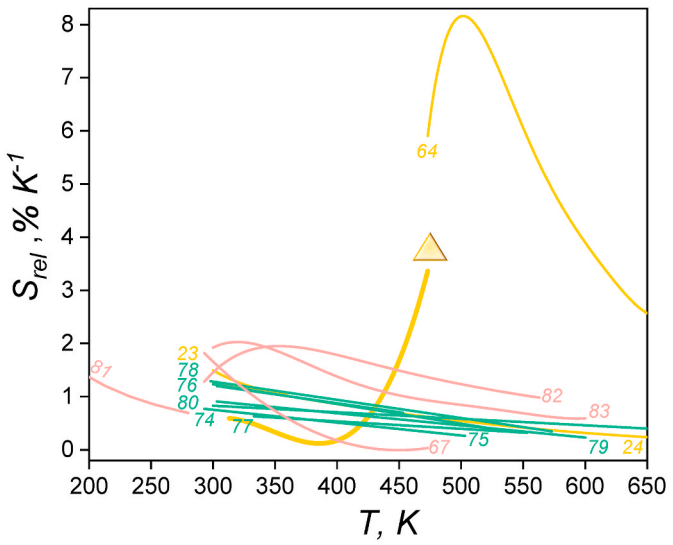

Fig. 4. Variation of the relative thermal sensitivity with the temperature for white light emitters (in gold thick line and shape of a triangle, are depicted the Ho^{3+}, Tm^{3+}:Y_2O_3 colloidal nanocrystals), green light emitters (in green lines) and other types of rare earth based thermometers operating in the visible region (in red lines). Numbers stand for the corresponding references. (For interpretation of the references to color in this figure legend, the reader is referred to the Web version of this article.)

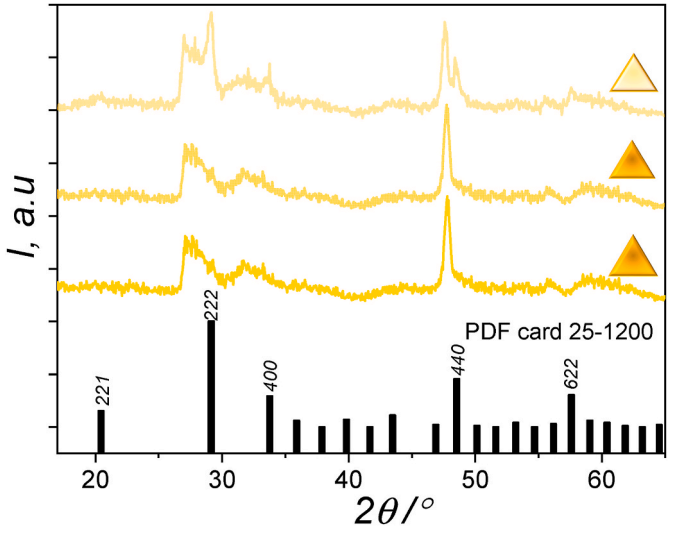

Fig. 5. XRPD patterns of Ho^{3+}, Tm^{3+}:Y_2O_3 colloidal nanocrystals, as synthesized (strong gold line), after only heating the nanocrystals (medium gold line) and after the white light experiments (faded gold line). The reference pattern of cubic Y_2O_3 (PDF card 25–1200) is included for comparison. The sketches within the figures stand for the shape of the particles. (For interpretation of the references to color in this figure legend, the reader is referred to the Web version of this article.)

473 K. For this model, an equation of the following form was applied:

$$\Delta = A + A_1 T + A_2 T^2 + A_3 T^3 \quad (1)$$

where A, A_1, A_2 and A_3 are constants to be determined from the fitting, and T stands for the absolute temperature. Having established the fitting equation, now we can analyze the thermometric performance of these nanocrystals by evaluating their absolute and relative thermal sensitivities, and their temperature resolution.

The absolute sensitivity would allow us to compare the performance of the three different luminescent nanothermometers we propose in this paper, since their temperature-dependence emission properties are recorded under the same conditions. It is defined as the first derivative of the intensity ratio [73]:

$$S_{abs} = \frac{\partial \Delta}{\partial T} \quad (2)$$

Using Eq. (1) that describes the evolution of intensity with temperature, we can determine the absolute sensitivity of the white light generated by these doped nanocrystals, as follows:

$$S_{abs} = A_1 + 2A_2 T + 3A_3 T^2 \quad (3)$$

On the other hand, the relative thermal sensitivity, used normally as a figure of merit to compare the performance of different thermometers, expresses the maximum change in the intensity ratio for each temperature degree and it is defined as [69]:

$$S_{rel} = \frac{1}{\Delta}\frac{\partial \Delta}{\partial T} x\ 100\% \quad (4)$$

This relative thermal sensitivity for our particular case is:

$$S_{rel} = \frac{A_1 + 2A_2 T + 3A_3 T^2}{A + A_1 T + A_2 T^2 + A_3 T^3} x100\% \quad (5)$$

And finally, the temperature resolution, defined as the smallest temperature change that can be resolved in a given measurement, is another parameter that can determine the thermometric performance of a thermometer, expressed as [69]:

$$\delta T = \frac{1}{S_{rel}}\frac{\delta \Delta}{\Delta} \quad (6)$$

where $\frac{\delta\Delta}{\Delta}$ stands for the uncertainty in the determination of the intensity ratio (0.5% in the common situations [69]). Hence, the smallest the value of δT, the better the thermometric performance of a thermometer.

Having determined the equations for S_{abs}, S_{rel} and δT, now we can compare the thermometric performance of Ho^{3+},Tm^{3+}:Y_2O_3 nanotriangles as a function of the particular wavelengths (blue, green and red) selected. The thermometric performance of these colloidal nanocrystals based on the third-order polynomial fitting model, as shown in Fig. 3 (c)–(e), reveals that the performance of the luminescent nanothermometer based on the red wavelength (in terms of S_{rel} and δT) is higher compared to the other two.

Concerning S_{rel}, the use of the red wavelength allows to have a higher sensitivity, 3.38% K^{-1} (Fig. 3 (e)), bigger than the ones that one can get by using the blue (0.41% K^{-1}), and green (2.38% K^{-1}) wavelengths at high temperature (473 K). δT evolution with the temperature, presented in Fig. 3 (f), emphasizes that the use of the red wavelength allows sensing temperature changes with more precision than by using the blue and green wavelengths.

The performance of Ho^{3+}, Tm^{3+}:Y_2O_3 colloidal nanocrystals as white light temperature sensors can be compared with other nano/micro materials operating *via* the principle of the white emissions or other types of luminescent thermometers operating in the visible region (Fig. 4). We are using for the comparison the maximum relative thermal sensitivity obtained by using the red wavelength in our work. Compared to other white light thermal sensors (all in gold line in Fig. 4) based on the blackbody radiation generated by the material when it is heated above a particular temperature, the performance of Ho^{3+},Tm^{3+}:Y_2O_3 nanocrystals is higher compared to other RE_2O_3 such as Er^{3+},Yb^{3+} doped Y_2O_3 particles [24], or Er^{3+}, Yb^{3+} doped Gd_2O_3 combined with Au NPs [23].

In materials such as transparent Nd^{3+} doped-oxyfluorotellurite (TZPN) glass host matrix [64], the performance of which was determined by the intensity ratio of the emission of the glass matrix (located at around 1480–1500 nm) and the emission of Nd^{3+} ions (located at around 1050–1070 nm), S_{rel} is up to 2-fold higher compared to our Ho^{3+},

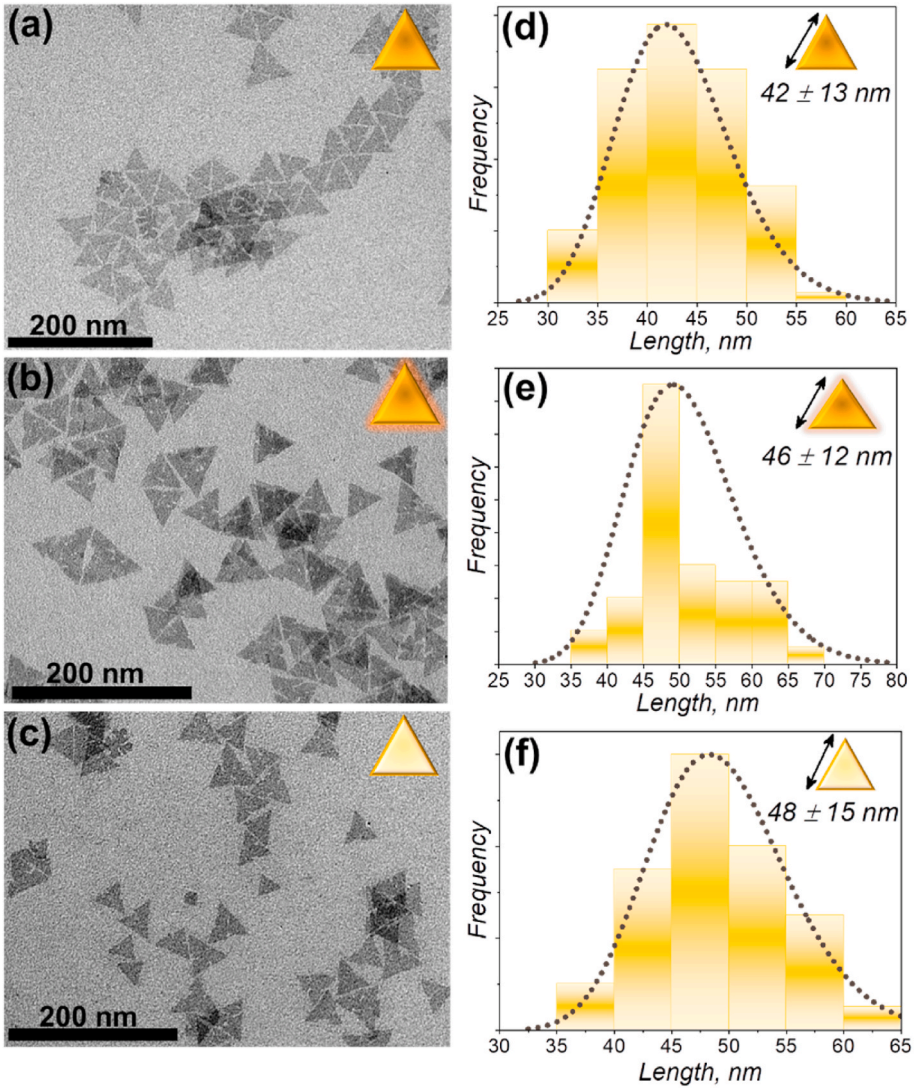

Fig. 6. TEM images and lognormal size distribution of the lateral length of Ho^{3+}, Tm^{3+}:Y_2O_3 nanocrystals: (a) and (d) as-synthesized; (b) and (e) after only heating the nanocrystals; (c) and (f) after the white light generation experiments. The sketches within the figures stand for the shape of the particles whereas the arrows in the size distribution graphs portray the parameter considered to determine their lengths.

Tm^{3+} doped Y_2O_3 nanocrystals (Fig. 4). Nevertheless, a key advantage of Ho^{3+}, Tm^{3+}:Y_2O_3 is the fact that it operates through a large temperature range, including as well the physiological one (310–473 K), whereas for the Nd^{3+} ion embedded in TZPN glass, operates in high temperatures above 473 K. In addition, the maximum sensitivity for Nd^{3+} ion embedded in TZPN, is reached at around 493 K, while as the temperature increases beyond 493 K, sensitivity continuously decreases, contrary to the example of Ho^{3+}, Tm^{3+} doped Y_2O_3 nanotriangles (Fig. 4). But the real advantage in our case is that we do not need to heat the material above a particular temperature to generate this white light, but we are generating it already at room temperature. Then, in the previous works reported in the literature, the white light was an artifact that affects to the reading mechanism used for lower temperatures (normally the luminescence intensity ratio between two emission peaks generated by the active lanthanide ion), and it has to be adapted to use these luminescent materials as luminescent thermometers at higher temperatures. Instead, in our case, this is the first time that white light generated at room temperature, and its variation as the temperature increases is used to determine temperature by luminescence means.

The performance of Ho^{3+}, Tm^{3+} doped Y_2O_3 can be compared also with other Er^{3+} green emissions-based thermometers (all in green color in Fig. 4). Clearly, the performance of our white light emitters is approximately 3-fold higher compared with those, including Er^{3+}, Yb^{3+} embedded in $GdVO_4$ [74], $NaY(WO_4)_2$ [75], $Gd_6O_5F_8$ [76], or $La_2Ti_2O_7$ [77]. In addition, it can be extracted from Fig. 4 that the performance of Ho^{3+}, Tm^{3+}:Y_2O_3 luminescent nanothermometers is higher compared to other green emitting Er^{3+}, Yb^{3+} doped in rare earth oxides (Y_2O_3 [78], Gd_2O_3 [79],or La_2O_3 [80]). The performance of other rare earth doped materials operating in the visible region (all in red color in Fig. 4) are relatively lower compared to Ho^{3+}, Tm^{3+} doped Y_2O_3 white thermal sensors. S_{rel} of these other materials, such as red emitters based on Eu^{3+} doped Y_2O_3 [81], or different Tm^{3+} based thermometers including single ($Tm,Yb:Sr_2GdF_7$ [82]) or dual emitting centers (Ho^{3+}, Tm^{3+}:$KLu(WO_4)_2$ [67], or Tm^{3+}, Er^{3+}, Yb^{3+}:$NaLuF_4$ [83]), is in the range of 2% K^{-1} (Fig. 4). From the comparison of all these data, it can be concluded that our white light emitters clearly portray luminescent thermometers with a high relative thermal sensitivity, which may inspire investigating potential application for these temperature sensors.

3.3. *Characterization of Ho^{3+} and Tm^{3+} doped Y_2O_3 colloidal nanocrystals*

We investigated the crystalline structure, the morphological characteristics (size and shape) and the functional groups attached to the

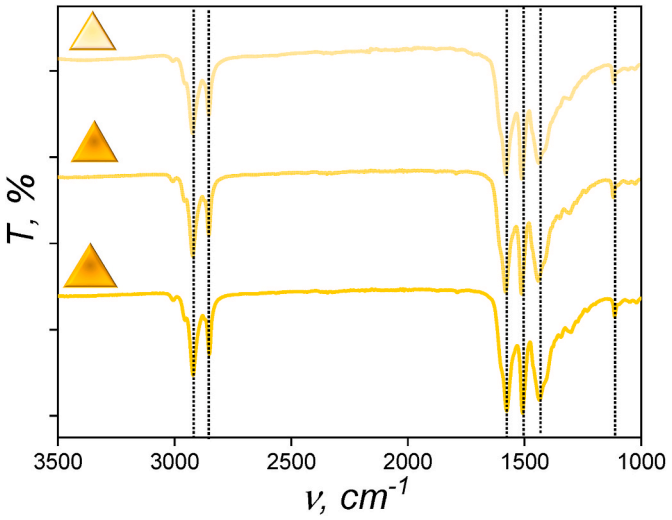

Fig. 7. FTIR analysis of Ho^{3+}, Tm^{3+}:Y_2O_3 nanocrystals as-synthesized (strong gold line), after only heating the nanocrystals (medium faded gold line) and after the white light generation experiments (strong faded gold line). The sketches within the figures stand for the shape of the particles. (For interpretation of the references to color in this figure legend, the reader is referred to the Web version of this article.)

surface of the Ho^{3+}, Tm^{3+}:Y_2O_3 colloidal nanocrystals, before and after generation of the white light. In addition, in order to distinguish if the observed effects are due to the laser exposure or the heating process, we mimicked the white light nanothermometric experiments, by exposing the colloidal nanocrystals in a heating plate for the same amount of time. The XRPD pattern of the as-synthesized nanocrystals by the thermal decomposition methodology display broad diffraction peaks, indicating poor crystallinity (Fig. 5, strong gold line). Nevertheless, some sharper peaks are detected, as well, that might be related to preferential growth orientations, as previously discussed [65].The pattern matched with the cubic crystalline structure of Y_2O_3 with space group *Ia* $\overline{3}$, with a slight shifting of the position of the diffraction peaks towards lower angles when compared to the reference pattern, as previously reported [65].

After the white light generation experiments, the data reveal that the crystallinity of the sample has improved (Fig. 5, strongly faded gold line), since the diffraction peaks appear sharper. Different new sharp peaks start to appear, mainly at the positions corresponding to the (222) and (440) planes, whereas the intensity of the (221), (400) and (622) peaks increased slightly. We presume that because of the high laser powers applied (a necessary condition for the white light generation), the heat provided to the sample lead to an improved degree of crystallinity. In previous examples of white light emitting Y_2O_3 particles reported in the literature [24,31–34], such structural investigation after the generation of the white light has not been conducted.

Finally, when the nanotriangles where exposed only to heat treatment, the crystalline pattern did not display any significant changes (Fig. 5, medium faded gold line). Logically, the XRPD pattern after heat treatment are expected to be similar with the one of the as-synthesized nanotriangles, since neither the organic surfactant that is coating the particles (oleic acid) cannot be removed at this temperature (the melting point is above 630 K) and either the host material Y_2O_3 exhibits any structural transformation within the room temperature to 473 K interval [84]. Hence, these clarifies that the main reason why the change of the crystalline profile is assigned to the laser exposure.

The size and shape of the colloidal nanocrystals were analyzed *via* TEM. Ho^{3+},Tm^{3+}:Y_2O_3 particles prepared by the thermal decomposition methodology display a triangular morphology (Fig. 6 (a)). Their average length size is ~43 ± 13 nm (Fig. 6 (d)), deduced after analyzing over 100 nanocrystals through the ImageJ software. The size and shape of the same particles exposed only to the heating treatment, does not exhibit any change in shape (Fig. 6 (b)), and the size of these particles is in the same range, although slightly larger (~46 ± 12 nm, Fig. 6 (e)), compared to the as the as-synthesized ones. After the white light generation experiments, the triangular shape of the particles is preserved (Fig. 6 (c)). On the other hand, it seems that their sizes are increased up to ~48 ± 15 nm (Fig. 6 (f)). Nevertheless, this difference is relatively small, and it is within the error of the measurement.

Finally, we recorded infrared spectra of these nanocrystals *via* FTIR spectroscopy, with the goal to study the presence of the coating organic surfactants on their surfaces. FTIR data, summarized in Fig. 7, demonstrate that there are no changes in the nanocrystals before (strong gold line), only during heating (faded gold line) or after the white light generation (strongly faded gold line) experiments, and that they are in all trails coated with oleic acid moieties. The absence of the typical vibrational bands of OLAC and OLAM such as the ν (C═O) stretching band located at 1710 cm^{-1} and the bending δ (NH_2) band located at 1595 cm^{-1}, and the presence of bands located at 1580 cm^{-1}, 1510 cm^{-1} and 1435 cm^{-1}, ascribed to the antisymmetric and symmetric stretching vibrations of the deprotonated carboxylic group (COO^-), respectively, indicate that the OLAC molecules were deprotonated and transformed into carboxylate anions, catalyzed by OLAM [85–87]. An additional observation that confirms that the nanocrystals after the white light generation experiments are coated with organic surfactant is their ability to be dispersed in apolar solvents, such as n-hexane.

4. Conclusions

In summary, we have reported the generation of white light emission from highly monodisperse oleic acid coated Ho^{3+}, Tm^{3+} doped Y_2O_3 colloidal nanotriangles, synthesized by thermal decomposition. We investigated different factors affecting the generation of white light emission, including the stability of the spectrum with time, the power of the laser applied, and the temperature at which the nanocrystals were exposed. Since the intensity of the emission of these Ho^{3+},Tm^{3+}:Y_2O_3 nanocrystals in the visible regime is highly dependent on the temperature, we explored their potential applicability as luminescent thermometers. These nanothermometers are highly sensitive to the change of temperature, exhibit high values of the relative thermal sensitivity (3.38% K^{-1}) and temperature resolution (0.15 K) at high temperatures (473 K), within the wavelength range from 400 to 750 nm. Finally, the effects of the high laser powers used for the excitation of these nanoparticles to generate white light on their crystalline structure, size, shape, and ligands attached to their surfaces have been analyzed.

Credit author statement

Albenc Nexha: Investigation, Conceptualization, Methodology, Data curation, Writing- Original draft preparation. **Maria Cinta Pujol**: Conceptualization, Writing - Review & Editing, Supervision. **Joan Josep Carvajal**: Conceptualization, Writing - Review & Editing, Supervision. **Francesc Díaz**: Funding acquisition and **Magdalena Aguiló**: Funding acquisition.

Declaration of competing interest

The authors declare that they have no known competing financial interests or personal relationships that could have appeared to influence the work reported in this paper.

Acknowledgements

This work was supported by the Spanish Government under projects MAT2016-75716-C2-1-R (AEI/FEDER, UE) and by the Generalitat de Catalunya under project 2017SGR755. A.N acknowledges financial support from the Generalitat de Catalunya under grant 2017FI_B00620, 2018FI_B100161 and 2019FI_B200154.

References

[1] K.T. Kamtekar, A.P. Monkman, M.R. Bryce, Recent advances in white organic light-emitting materials and devices (WOLEDs), Adv. Mater. 22 (2010) 572–582.

[2] S.H. Kim, S. Park, J.E. Kwon, S.Y. Park, Organic light-emitting diodes with a white-emitting molecule: emission mechanism and device characteristics, Adv. Funct. Mater. 21 (2011) 644–651.

[3] J. Wang, T. Ming, Z. Jin, J. Wang, L.D. Sun, C.H. Yan, Photon energy upconversion through thermal radiation with the power efficiency reaching 16, Nat. Commun. 5 (2014) 5669–5678.

[4] J. Wu, G. Zheng, X. Liu, J. Qiu, Near-infrared laser driven white light continuum generation: materials, photophysical behaviours and applications, Chem. Soc. Rev. 49 (2020) 3461–3483.

[5] C. Wang, S. Xu, Y. Wang, Z. Wang, Y. Cui, Aqueous synthesis of multilayer Mn:ZnSe/Cu:ZnS quantum dots with white light emission, J. Mater. Chem. C 2 (2014) 660–666.

[6] M.J. Bowers, J.R. McBride, S.J. Rosenthal, White-light emission from magic-sized cadmium selenide nanocrystals, J. Am. Chem. Soc. 127 (2005) 15378–15379.

[7] W.J. Zhang, C.Y. Pan, F. Cao, H. Wang, X. Yang, Highly bright and stable white-light-emitting cadmium-free Ag,Mn co-doped Zn-In-S/ZnS quantum dots and their electroluminescence, J. Mater. Chem. C 6 (2018) 10233–10240.

[8] S.K. Panda, S.G. Hickey, H.V. Demir, A. Eychmüller, Bright white-light emitting manganese and copper Co-doped ZnSe quantum dots, Angew. Chem. Int. Ed. 50 (2011) 4432–4436.

[9] H.S. Chen, H.Y. Hong, R.V. Kumar, White light emission from semiconductor nanocrystals by in situ colour tuning in an alternating thermodynamic-kinetic fashion, J. Mater. Chem. 21 (2011) 5928–5932.

[10] M.M. Krause, J. Mooney, P. Kambhampati, Chemical and thermodynamic control of the surface of semiconductor nanocrystals for designer white light emitters, ACS Nano 7 (2013) 5922–5929.

[11] S. Sapra, S. Mayilo, T.A. Klar, A.L. Rogach, J. Feldmann, Bright white-light emission from semiconductor nanocrystals: by chance and by design, Adv. Mater. 19 (2007) 569–572.

[12] E.L. Williams, K. Haavisto, J. Li, G.E. Jabbour, Excimer-based white phosphorescent organic light-emitting diodes with nearly 100 % internal quantum efficiency, Adv. Mater. 19 (2007) 197–202.

[13] K. Sakai, T. Ishikawa, T. Akutagawa, A blue-white-yellow color-tunable excited state intramolecular proton transfer (ESIPT) fluorophore: sensitivity to polar-nonpolar solvent ratios, J. Mater. Chem. C 1 (2013) 7866–7871.

[14] N. Nagarajan, G. Velmurugan, A. Prakash, N. Shakti, M. Katiyar, P. Venuvanalingam, R. Renganathan, Highly emissive luminogens based on imidazo[1,2-a]pyridine for electroluminescent applications, Chem, Asian J 9 (2014) 294–304.

[15] J. Luo, X. Li, Q. Hou, J.B. Peng, W. Yang, Y. Cao, High-efficiency white-light emission from a single copolymer: fluorescent blue, green, and red chromophores on a conjugated polymer backbone, Adv. Mater. 19 (2007) 1113–1117.

[16] H. Wu, G. Zhou, J. Zou, C.L. Ho, W.Y. Wong, W. Yang, J. Peng, Y. Cao, Efficient polymer white-light-emitting devices for solid-state lighting, Adv. Mater. 21 (2009) 4181–4184.

[17] E. Ravindran, N. Somanathan, Efficient white-light emission from a single polymer system with “spring-like” self-assemblies induced emission enhancement and intramolecular charge transfer characteristics, J. Mater. Chem. C 5 (2017) 4763–4774.

[18] O. Sahin, M.E. Cinar, E. Tekin, S.P. Mucur, S. Topal, G. Suna, M.S. Eroglu, T. Ozturk, White light emitting polymers possessing thienothiophene and boron units, ChemistrySelect 2 (2017) 2889–2894.

[19] A. Balamurugan, M.L.P. Reddy, M. Jayakannan, Single polymer photosensitizer for Tb^{3+} and Eu^{3+} ions: an approach for white light emission based on carboxylic-functionalized poly(m-phenylenevinylene)s, J. Phys. Chem. B 113 (2009) 14128–14138.

[20] Q. Tang, S. Liu, Y. Liu, D. He, J. Miao, X. Wang, Y. Ji, Z. Zheng, Color tuning and white light emission via in situ doping of luminescent lanthanide metal-organic frameworks, Inorg. Chem. 53 (2014) 289–293.

[21] G. He, D. Guo, C. He, X. Zhang, X. Zhao, C. Duan, A color-tunable europium complex emitting three primary colors and white light, Angew. Chem. Int. Ed. 48 (2009) 6132–6135.

[22] X. Ma, X. Li, Y.E. Cha, L.P. Jin, Highly thermostable one-dimensional lanthanide (III) coordination polymers constructed from benzimidazole-5,6-dicarboxylic acid and 1,10-phenanthroline: synthesis, structure, and tunable white-light emission, Cryst. Growth Des. 12 (2012) 5227–5232.

[23] M.L. Debasu, D. Ananias, I. Pastoriza-Santos, L.M. Liz-Marzán, J. Rocha, L. D. Carlos, All-in-one optical heater-thermometer nanoplatform operative from 300 to 2000 K based on Er^{3+} emission and blackbody radiation, Adv. Mater. 25 (2013) 4868–4874.

[24] M. Łukaszewicz, R. Tomala, R. Lisiecki, From upconversion to thermal radiation: spectroscopic properties of a submicron Y_2O_3:Er^{3+},Yb^{3+} ceramic under IR excitation in an extremely broad temperature range, J. Mater. Chem. C 8 (2020) 1072–1082.

[25] Z. Mao, D. Wang, Q. Lu, W. Yu, Z. Yuan, Tunable single-doped single-host full-color-emitting $LaAlO_3$:Eu phosphorvia valence state-controlled means, Chem. Commun. (2009) 346–348.

[26] L. Xing, W. Yang, J. Lin, M. Huang, Y. Xue, Enhanced and stable upconverted white-light emission in Ho^{3+}/Yb^{3+}/Tm^{3+}-doped $LiNbO_3$ single crystal via Mg^{2+} ion doping, Sci. Rep. 7 (2017) 14725.

[27] T. Wang, H. Yu, C.K. Siu, J. Qiu, X. Xu, S.F. Yu, White-light whispering-gallery-mode lasing from lanthanide-doped upconversion $NaYF_4$ hexagonal microrods, ACS Photonics 4 (2017) 1539–1543.

[28] N.S. Singh, N.K. Sahu, D. Bahadur, Multicolor tuning and white light emission from lanthanide doped $YPVO_4$ nanorods: energy transfer studies, J. Mater. Chem. C 2 (2014) 548–555.

[29] E.W. Barrera, M.C. Pujol, J.J. Carvajal, X. Mateos, R. Solé, J. Massons, A. Speghini, M. Bettinelli, C. Cascales, M. Aguiló, F. Díaz, White light upconversion in Yb-sensitized (Tm, Ho)-doped $KLu(WO_4)_2$ nanocrystals: the effect of Eu incorporation, Phys. Chem. Chem. Phys. 16 (2014) 1679–1686.

[30] L. Marciniak, W. Strek, D. Hreniak, Y. Guyot, Temperature of broadband anti-Stokes white emission in $LiYbP_4O_{12}$:Er nanocrystals, Appl. Phys. Lett. 105 (2014) 173113–173117.

[31] G. Bilir, B. Di Bartolo, Production of bright, wideband white light from Y_2O_3 nano-powders induced by laser diode emission, Opt. Mater. 36 (2014) 1357–1360.

[32] G. Bilir, G. Özen, J. Collins, M. Cesaria, B. Di Bartolo, Unconventional production of bright white light emission by Nd-doped and nominally un-doped Y_2O_3 nano-powders, IEEE Photonics J 6 (2014) 8200518–8200535.

[33] M. Cesaria, J. Collins, B. Di Bartolo, On the efficient warm white-light emission from nano-sized Y_2O_3, J. Lumin. 169 (2016) 574–580.

[34] C. Lin, C. Zhang, J. Lin, Sol-gel derived Y_2O_3 as an efficient bluish-white phosphor without metal activator ions, J. Lumin. 129 (2009) 1469–1474.

[35] S. Tabanli, G. Eryurek, B. Di Bartolo, White light emission from Er_2O_3 nano-powder excited by infrared radiation, Opt. Mater. 69 (2017) 207–213.

[36] J. Wang, J.H. Hao, P.A. Tanner, Persistent luminescence upconversion for Er_2O_3 under 975 nm excitation in vacuum, J. Lumin. 164 (2015) 116–122.

[37] S. Tabanli, H.C. Yilmaz, G. Bilir, M. Erdem, G. Eryurek, B. Di Bartolo, J. Collins, Broadband, white light emission from doped and undoped insulators, ECS J. Solid State Sci. Technol. 7 (2018) 3199–3210.

[38] J. Wang, P.A. Tanner, Upconversion for white light generation by a single compound, J. Am. Chem. Soc. 132 (2009) 947–949.

[39] J. Wang, J.H. Hao, P.A. Tanner, Luminous and tunable white-light upconversion for YAG ($Yb_3Al_5O_{12}$) and $(Yb,Y)_2O_3$ nanopowders, Opt. Lett. 35 (2010) 3922–3924.

[40] M. Jayasimhadri, B.V. Ratnam, K. Jang, H.S. Lee, S.S. Yi, J.H. Jeong, Conversion of green emission into white light in Gd_2O_3 nanophosphors, Thin Solid Films 518 (2010) 6210–6213.

[41] G. Bilir, O. Erguzel, Up-conversion emission properties and unexpected white light emission from Er^{3+}/Yb^{3+} doped Gd_2O_3 nanophosphors, Mater. Res. Express 3 (2016) 106201–106213.

[42] A. Singh, S. Singh, D. Kumar, D. Rai, S. Rai, K. Kumar, Light-into-heat conversion in La_2O_3:Er^{3+}-Yb^{3+} phosphor: an incandescent emission, Opt. Lett. 37 (2012) 776–778.

[43] C.I. Silva Filho, A.L. Oliveira, S.C.F. Pereira, G.F. de Sá, L.L. da Luz, S. Alves, Bright thermal (blackbody) emission of visible light from LnO_2 (Ln=Pr, Tb), photoinduced by a NIR 980 nm laser, Dalton Trans. 48 (2019) 2574–2581.

[44] T. Paik, T.R. Gordon, A.M. Prantner, H. Yun, C.B. Murray, Designing tripodal and triangular gadolinium oxide nanoplates and self-assembled nanofibrils as potential multimodal bioimaging probes, ACS Nano 7 (2013) 2850–2859.

[45] E. Hemmer, N. Venkatachalam, H. Hyodo, A. Hattori, Y. Ebina, H. Kishimoto, K. Soga, Upconverting and NIR emitting rare earth based nanostructures for NIR-bioimaging, Nanoscale 5 (2013) 11339–11361.

[46] H. Dong, S.R. Du, X.Y. Zheng, G.M. Lyu, L.D. Sun, L.D. Li, P.Z. Zhang, C. Zhang, C. H. Yan, Lanthanide nanoparticles: from design toward bioimaging and therapy, Chem. Rev. 115 (2015) 10725–10815.

[47] R.D. Teo, J. Termini, H.B. Gray, Lanthanides: applications in cancer diagnosis and therapy, J. Med. Chem. 59 (2016) 6012–6024.

[48] J.Y. Park, Y. Chang, G.H. Lee, Multi-modal imaging and cancer therapy using lanthanide oxide nanoparticles: current status and perspectives, Curr. Med. Chem. 22 (2015) 569–581.

[49] Y. Peng, X. Chen, Z. Gao, Determination of trace amounts of mercury using hierarchically nanostructured europium oxide, Talanta 82 (2010) 1924–1928.

[50] M.L. Debasu, H. Oliveira, J. Rocha, L.D. Carlos, Colloidal $(Gd_{0.98}Nd_{0.02})_2O_3$ nanothermometers operating in a cell culture medium within the first and second biological windows, J. Rare Earths 38 (2020) 483–491.

[51] L. Aguilar-Vázquez, M.P. Aguilar-Caballos, A. Gómez-Hens, Development of an automatic high-throughput assay for tetracycline determination by using Eu_2O_3 nanoparticles and dry-reagent technology, Talanta 119 (2014) 111–115.

[52] Z. Chen, H. Jia, K. Sharafudeen, W. Dai, Y. Liu, G. Dong, J. Qiu, Up-conversion luminescence from single vanadate through blackbody radiation harvesting broadband near-infrared photons for photovoltaic cells, J. Alloys Compd. 663 (2016) 204–210.

[53] Y. Zhu, W. Xu, C. Li, H. Zhang, B. Dong, L. Xu, S. Xu, H. Song, Broad white light and infrared emission bands in YVO_4:Yb^{3+},Ln^{3+} (Ln^{3+}=Er^{3+}, Tm^{3+}, or Ho^{3+}), Appl. Phys. Express 5 (2012) 92701–92704.

[54] C. Miao, T. Liu, Y. Zhu, Q. Dai, W. Xu, L. Xu, S. Xu, Y. Zhao, H. Song, Super-intense white upconversion emission of Yb_2O_3 polycrystals and its application on luminescence converter of dye-sensitized solar cells, Opt. Lett. 38 (2013) 3340–3343.

[55] A. Joshi, Y.A. Sharaby, S.S. Hassan, Temperature-induced optical bistability with Kerr-nonlinear blackbody reservoir, Opt Commun. 359 (2016) 387–392.

[56] S.M. Redmond, S.C. Rand, S.L. Oliveira, Bistable emission of a black-body radiator, Appl. Phys. Lett. 85 (2004) 5517–5519.

[57] S. Redmond, S.C. Rand, X.L. Ruan, M. Kaviany, Multiple scattering and nonlinear thermal emission of Yb^{3+}, Er^{3+}:Y_2O_3 nanopowders, J. Appl. Phys. 95 (2004) 4069–4077.

[58] F. Vetrone, J.C. Boyer, J.A. Capobianco, A. Speghini, M. Bettinelli, Effect of Yb^{3+} codoping on the upconversion emission in nanocrystalline Y_2O_3:Er^{3+}, J. Phys. Chem. B 107 (2003) 1107–1112.
[59] A.O.G. Dikovska, P.A. Atanasov, M. Jiménez de Castro, A. Perea, J. Gonzalo, C. N. Afonso, J. García López, Optically active Er^{3+}-Yb^{3+} codoped Y_2O_3 films produced by pulsed laser deposition, Thin Solid Films 500 (2006) 336–340.
[60] Y. Sato, J. Akiyama, T. Taira, Effects of rare-earth doping on thermal conductivity in $Y_3Al_5O_{12}$ crystals, Opt. Mater. 31 (2009) 720–724.
[61] H. Zhou, D. Yi, Effect of rare earth doping on thermo-physical properties of lanthanum zirconate ceramic for thermal barrier coatings, J. Rare Earths 26 (2008) 770–774.
[62] G. Bilir, G. Eryürek, The role played by dopant ions for the production of broadband white light emission from metal oxide nano-powders under laser diode excitation, Ceram. Int. 42 (2016) 6065–6071.
[63] A. Nexha, J.J. Carvajal, M.C. Pujol Baiges, F. Díaz, M. Aguiló, Lanthanide doped luminescence nanothermometers in the biological windows: strategies and applications, Nanoscale 13 (2021) 7913–7987.
[64] L. Marciniak, K. Trejgis, R. Lisiecki, A. Bednarkiewicz, Synergy between NIR luminescence and thermal emission toward highly sensitive NIR operating emissive thermometry, Sci. Rep. 10 (2020) 19692–19699.
[65] D. Wang, Y. Kang, X. Ye, C.B. Murray, Mineralizer-assisted shape-control of rare earth oxide nanoplates, Chem. Mater. 26 (2014) 6328–6332.
[66] A. Nexha, J.J. Carvajal, M.C. Pujol, F. Díaz, M. Aguiló, Short-wavelength infrared self-assessed photothermal agents based on Ho,Tm:$KLu(WO_4)_2$ nanocrystals operating in the third biological window (1.45-1.96 μm wavelength range), J. Mater. Chem. C 8 (2020) 180–191.
[67] A. Nexha, J.J. Carvajal, M.C. Pujol, F. Díaz, M. Aguiló, Synthesis of monoclinic Ho, Tm:$KLu(WO_4)_2$ microrods with high photothermal conversion efficiency via a thermal decomposition-assisted method, J. Mater. Chem. C 9 (2021) 2024–2036.
[68] A. Nexha, M.C. Pujol, J.J. Carvajal, F. Díaz, M.J.N. Aguiló, Effect of the size and shape of Ho, Tm:KLu $(WO_4)_2$ nanoparticles on their self-assessed photothermal properties, Nanomaterials 11 (2021) 485–511.
[69] C.D.S. Brites, A. Millán, L.D. Carlos, Handb. Phys. Chem. Rare Earths 49 (2016) 339–427 (Chapter 281).
[70] D. Jaque, F. Vetrone, Luminescence nanothermometry, Nanoscale 4 (2012) 4301–4326.
[71] O.A. Savchuk, J.J. Carvajal, C. Cascales, M. Aguiló, F. Díaz, Benefits of silica core-shell structures on the temperature sensing properties of Er,Yb:$GdVO_4$ up-conversion nanoparticles, ACS Appl. Mater. Interfaces 8 (2016) 7266–7273.
[72] O.A. Savchuk, J.J. Carvajal, J. Massons, C. Cascales, M. Aguiló, F. Díaz, Novel low-cost, compact and fast signal processing sensor for ratiometric luminescent nanothermometry, Sens. Actuators A Phys. 250 (2016) 87–95.
[73] P.V.d. Santos, M.T.d. Araujo, A.S. Gouveia-Neto, J.A.M. Neto, A.S.B. Sombra, Optical temperature sensing using upconversion fluorescence emission in Er^{3+}/Yb^{3+}-codoped chalcogenide glass, Appl. Phys. Lett. 73 (1998) 578–580.
[74] N.M. Bhiri, M. Dammak, M. Aguiló, F. Díaz, J.J. Carvajal, M.C. Pujol, Stokes and anti-Stokes operating conditions dependent luminescence thermometric performance of Er^{3+}-doped and Er^{3+}, Yb^{3+} co-doped $GdVO_4$ microparticles in the non-saturation regime, J. Alloys Compd. 814 (2020) 152197–152211.
[75] M. Lin, L. Xie, Z. Wang, B.S. Richards, G. Gao, J. Zhong, Facile synthesis of monodisperse sub-20 nm $NaY(WO_4)_2$:Er^{3+},Yb^{3+} upconversion nanoparticles: a new choice for nanothermometry, J. Mater. Chem. C 7 (2019) 2971–2977.
[76] S. Du, X. Ma, Q. Qiang, G. Zhang, Y. Wang, Emission in $Gd_6O_5F_8$:Yb^{3+},Er^{3+} microparticles for multimodal luminescence and temperature sensing upon 980 nm excitation, Phys. Chem. Chem. Phys. 18 (2016) 26894–26899.
[77] Y. Liu, G. Bai, E. Pan, Y. Hua, L. Chen, S. Xu, Upconversion fluorescence property of Er^{3+}/Yb^{3+} codoped lanthanum titanate microcrystals for optical thermometry, J. Alloys Compd. 822 (2020) 153449–153456.
[78] R.G. Geitenbeek, B.B.V. Salzmann, A.E. Nieuwelink, A. Meijerink, B. M. Weckhuysen, Chemically and thermally stable lanthanide-doped Y_2O_3 nanoparticles for remote temperature sensing in catalytic environments, Chem. Eng. Sci. 198 (2019) 235–240.
[79] S.K. Singh, K. Kumar, S.B. Rai, Er^{3+}/Yb^{3+} codoped Gd_2O_3 nano-phosphor for optical thermometry, Sens. Actuators A Phys. 149 (2009) 16–20.
[80] R. Dey, V.K. Rai, Yb^{3+} sensitized Er^{3+} doped La_2O_3 phosphor in temperature sensors and display devices, Dalton Trans. 43 (2014) 111–118.
[81] A.S. Souza, L.A.O. Nunes, I.G.N. Silva, F.A.M. Oliveira, L.L. da Luz, H.F. Brito, M.C. F.C. Felinto, R.A.S. Ferreira, S.A. Júnior, L.D. Carlos, O.L. Malta, Highly-sensitive Eu^{3+} ratiometric thermometers based on excited state absorption with predictable calibration, Nanoscale 8 (2016) 5327–5333.
[82] W. Chen, J. Cao, F. Hu, R. Wei, L. Chen, H. Guo, Sr_2GdF_7:Tm^{3+}/Yb^{3+} glass ceramic: a highly sensitive optical thermometer based on FIR technique, J. Alloys Compd. 735 (2018) 2544–2550.
[83] H. Lu, H. Hao, G. Shi, Y. Gao, R. Wang, Y. Song, Y. Wang, X. Zhang, Optical temperature sensing in β-$NaLuF_4$:Yb^{3+}/Er^{3+}/Tm^{3+} based on thermal, quasi-thermal and non-thermal coupling levels, RSC Adv. 6 (2016) 55307–55311.
[84] N. Pinna, G. Garnweitner, P. Beato, M. Niederberger, M. Antonietti, Synthesis of yttria-based crystalline and lamellar nanostructures and their formation mechanism, Small 1 (2005) 112–121.
[85] L. Zhang, R. He, H.C. Gu, Oleic acid coating on the monodisperse magnetite nanoparticles, Appl. Surf. Sci. 253 (2006) 2611–2617.
[86] M. Klokkenburg, J. Hilhorst, B.H. Erné, Surface analysis of magnetite nanoparticles in cyclohexane solutions of oleic acid and oleylamine, Vib. Spectrosc. 43 (2007) 243–248.
[87] R.A. Harris, P.M. Shumbula, H. van der Walt, Analysis of the interaction of surfactants oleic acid and oleylamine with iron oxide nanoparticles through molecular mechanics modeling, Langmuir 31 (2015) 3934–3943.